Electronic Supplementary Material (ESI) for Nanoscale.

Mo-X_4 (X= O, NH and S) mediated triphenylene-based two-dimensional carbon-rich conjugate frameworks for efficient nitrogen reduction reaction

Man Qiao,[a,*] *Jiachi Xie,*[a] *and Dongdong Zhu* [a,*]

[a] School of Chemistry and Materials Science, Institute of Advanced Materials and Flexible Electronics (IAMFE), Nanjing University of Information Science and Technology, Nanjing 210044, Jiangsu, China E-mail: dd.zhu@nuist.edu.cn, qiaoman@nuist.edu.cn

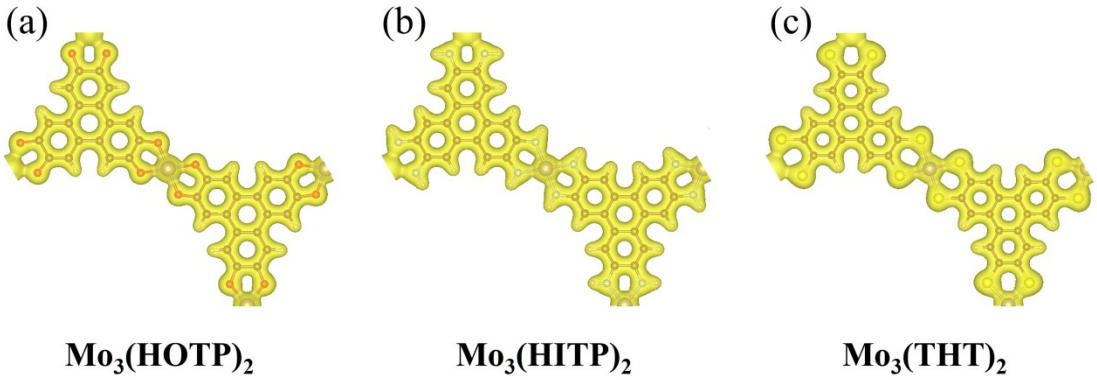

Figure S1. The charge density distribution of (a) $Mo_3(HOTP)_2$, (b) $Mo_3(HITP)_2$ and (c) $Mo_3(THT)_2$ monolayer.

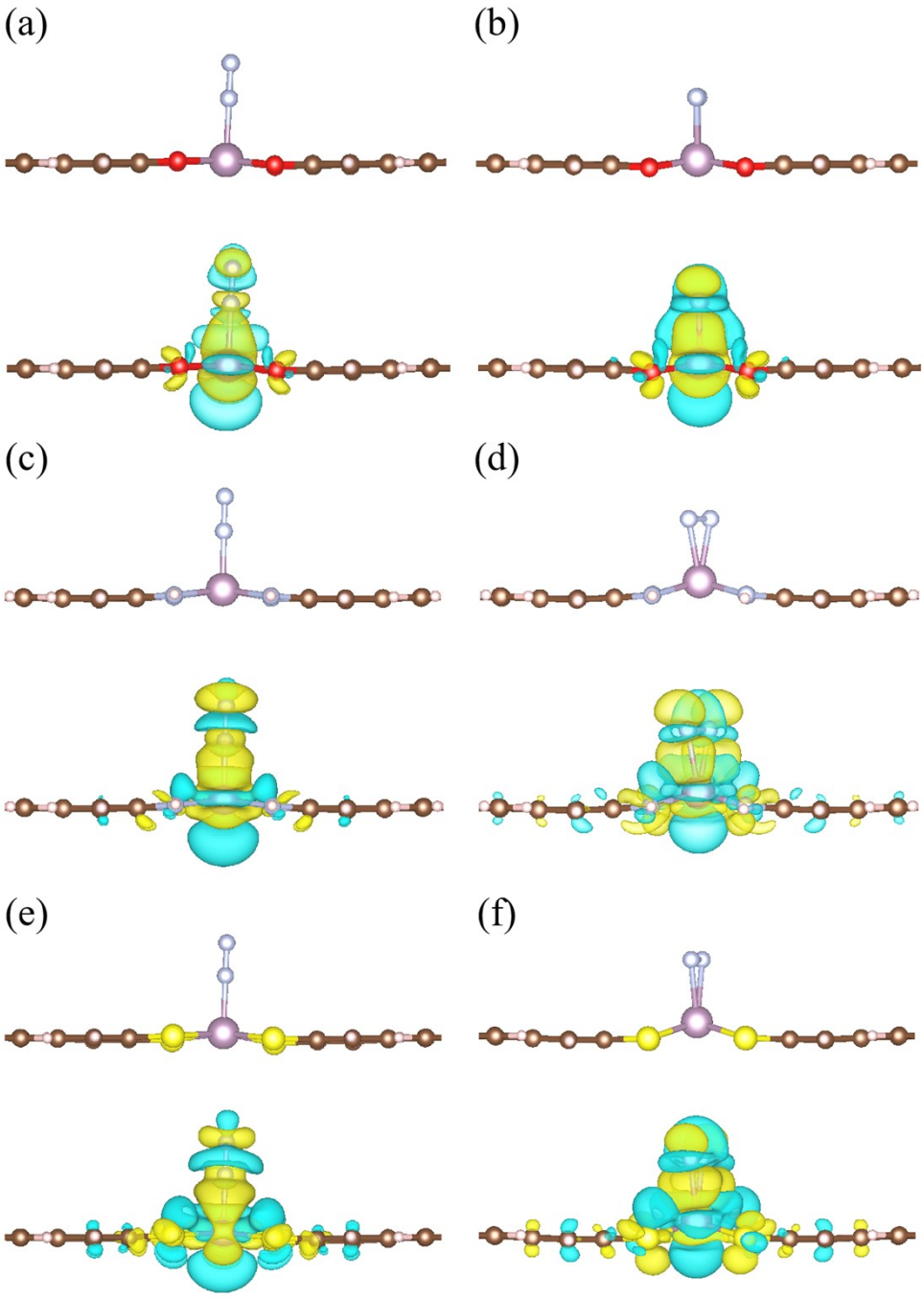

Figure S2. Schematics of the (a, c, e) end-on and (b, d, f) side-on configuration and the corresponding charge density difference distribution for N_2 adsorption on (a, b) $Mo_3(HOTP)_2$, (c, d) $Mo_3(HITP)_2$ and (e, f) $Mo_3(THT)_2$surface. Positive and negative charges are shown in yellow and light green color, respectively.

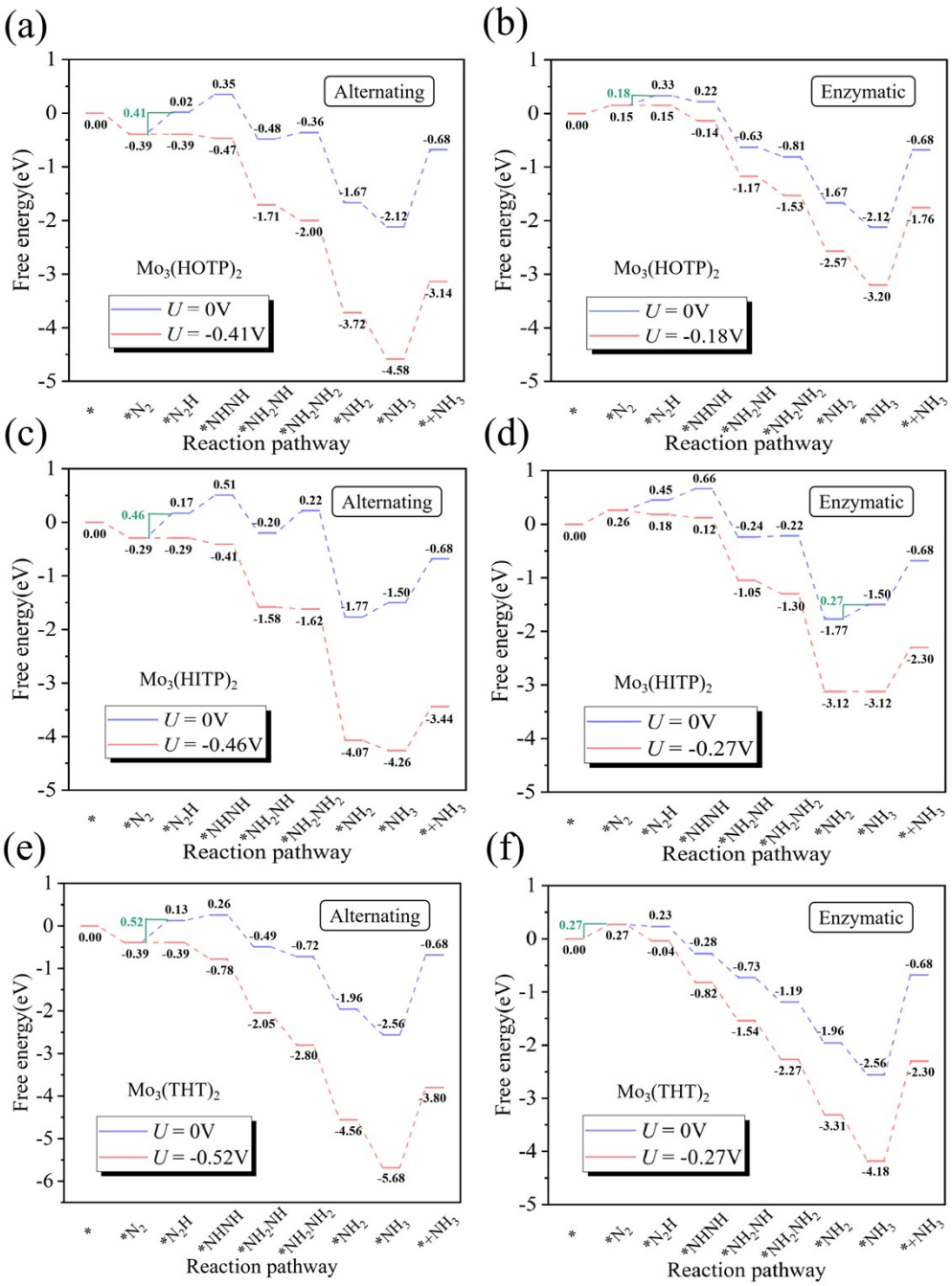

Figure S3. Gibbs free energy diagrams for NRR on $Mo_3(HOTP)_2$, $Mo_3(HITP)_2$ and $Mo_3(THT)_2$ surface through the alternating and enzymatic pathway at zero (blue lines) and applied potential (red lines). The Gibbs free energy change for each process is marked below the horizontal bar, and the ΔG_{PDS} is highlighted in green.

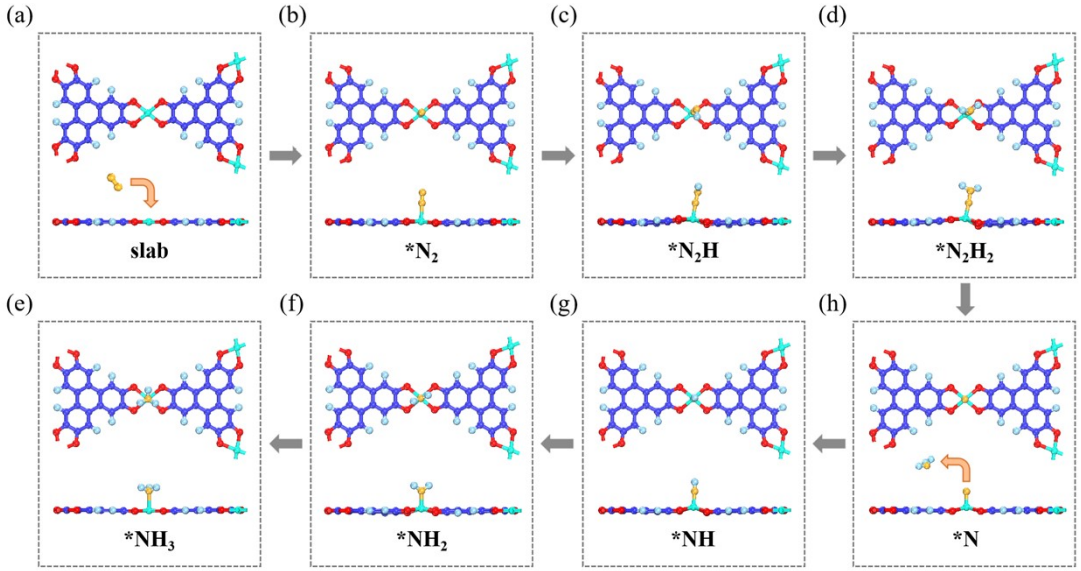

Figure S4. The top and the side views of optimized configurations of different NRR intermediates in the distal pathway on $Mo_3(HOTP)_2$ surface.

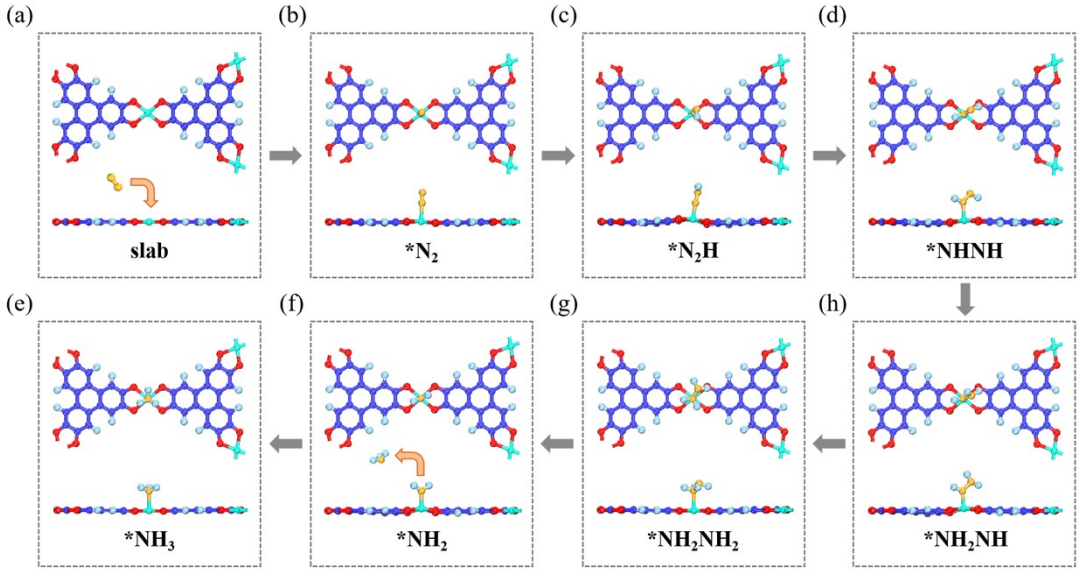

Figure S5. The top and the side views of optimized configurations of different NRR intermediates in the alternating pathway on $Mo_3(HOTP)_2$ surface.

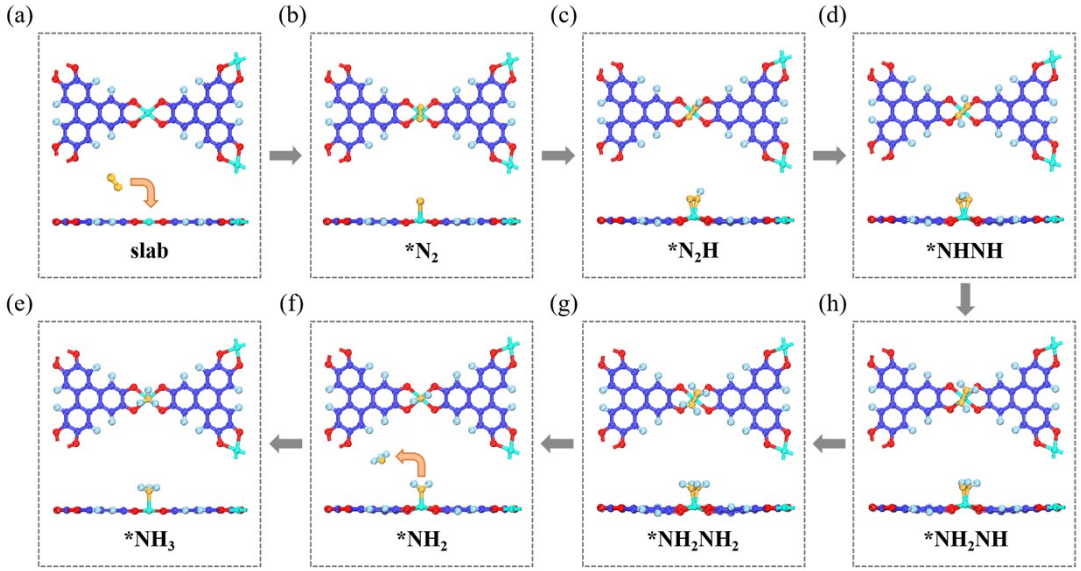

Figure S6. The top and the side views of optimized configurations of different NRR intermediates in the enzymatic pathway on $Mo_3(HOTP)_2$ surface.

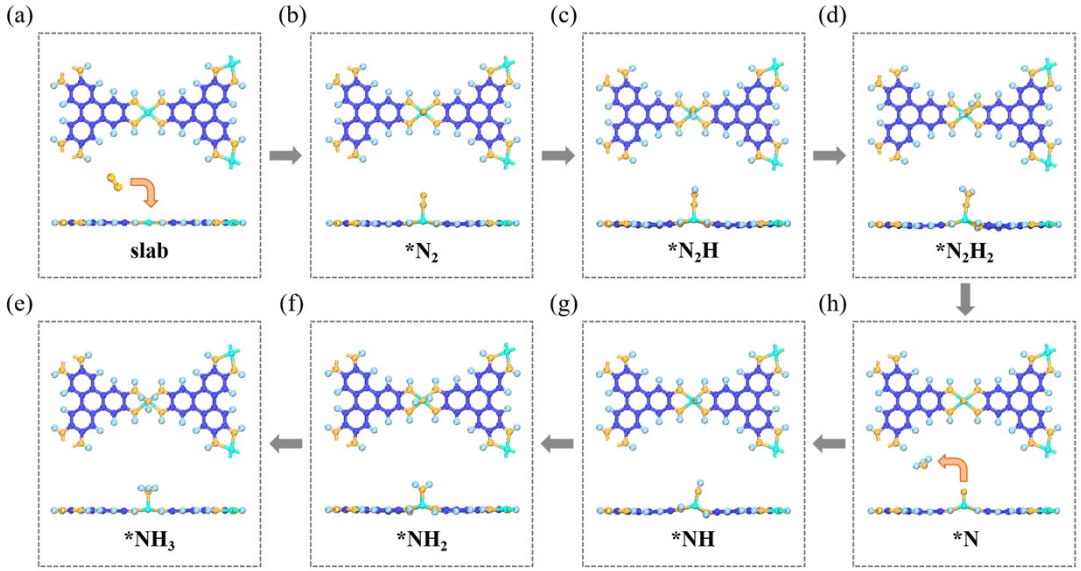

Figure S7. The top and the side views of optimized configurations of different NRR intermediates in the distal pathway on $Mo_3(HITP)_2$ surface.

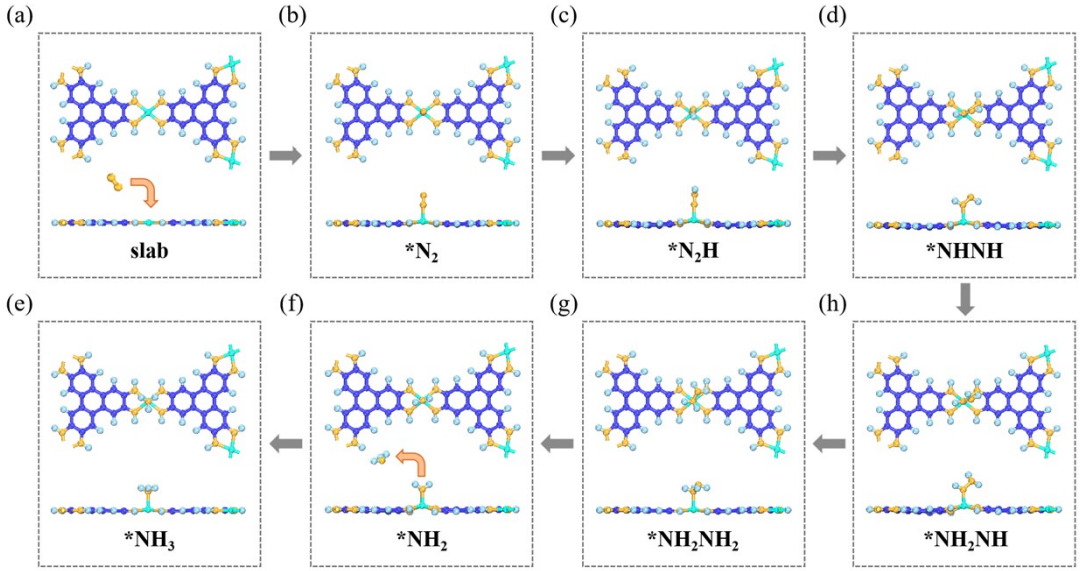

Figure S8. The top and the side views of optimized configurations of different NRR intermediates in the alternating pathway on $Mo_3(HITP)_2$ surface.

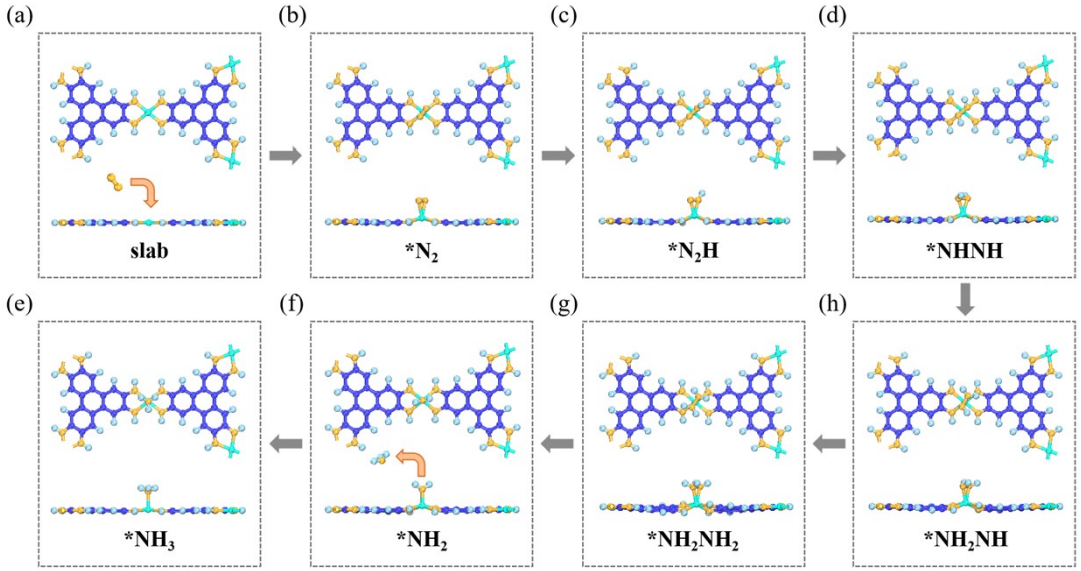

Figure S9. The top and the side views of optimized configurations of different NRR intermediates in the enzymatic pathway on $Mo_3(HITP)_2$ surface.

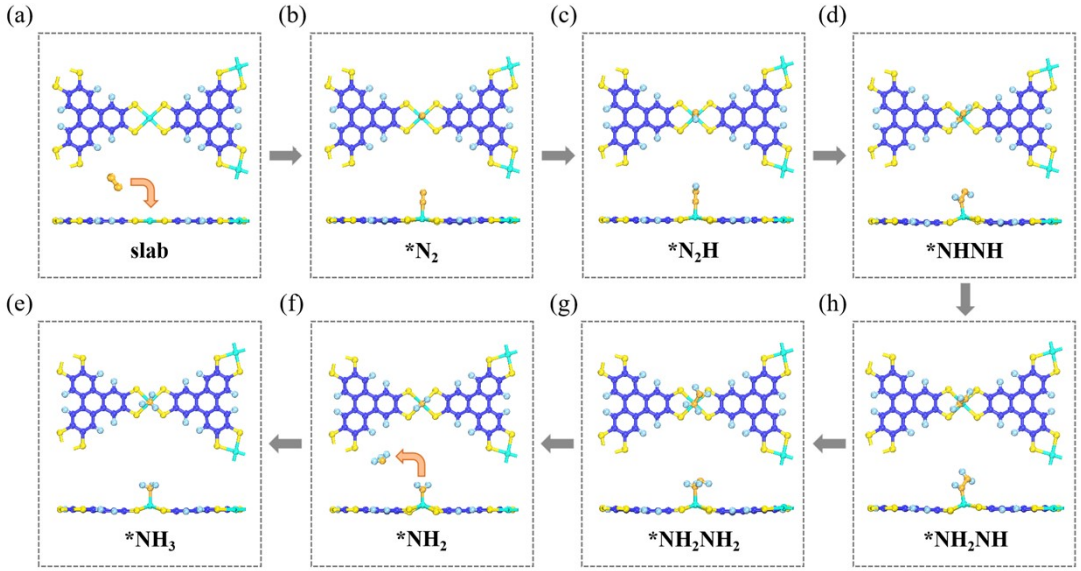

Figure S10. The top and the side views of optimized configurations of different NRR intermediates in the distal pathway on $Mo_3(THT)_2$ surface.

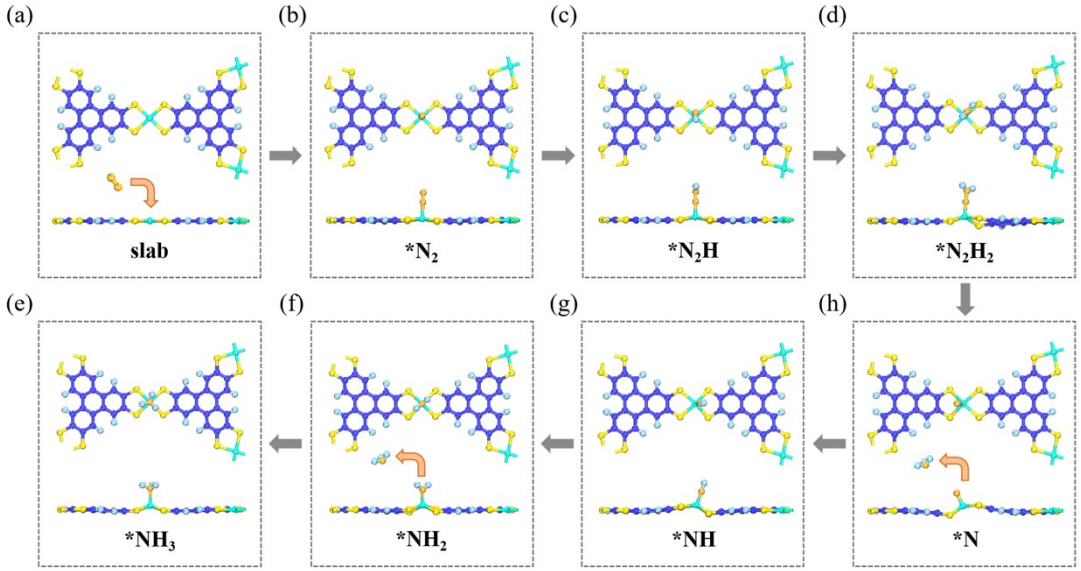

Figure S11. The top and the side views of optimized configurations of different NRR intermediates in the alternating pathway on $Mo_3(THT)_2$ surface.

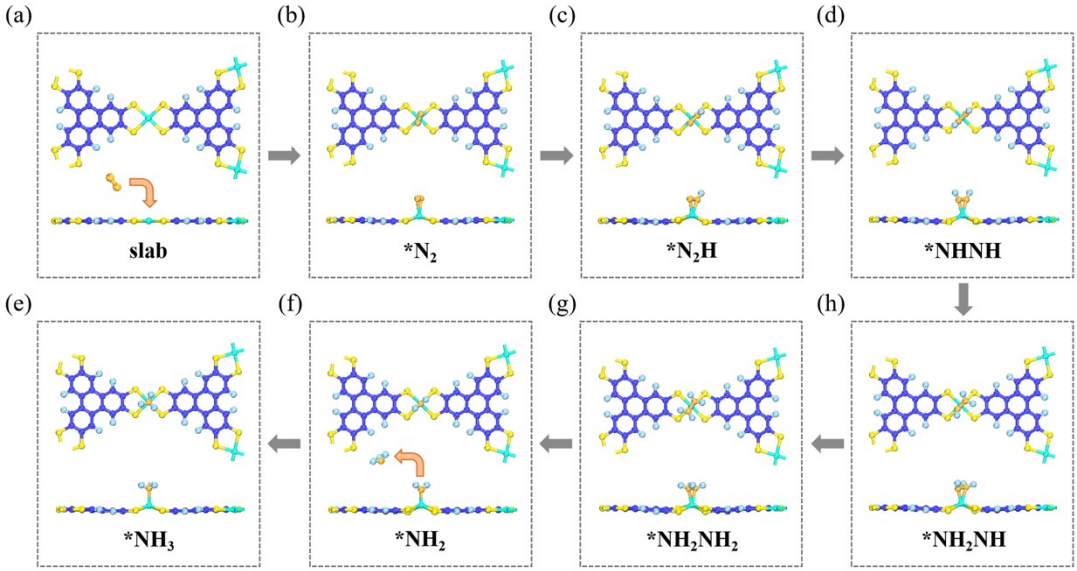

Figure S12. The top and the side views of optimized configurations of different NRR intermediates in the enzymatic pathway on $Mo_3(THT)_2$ surface.

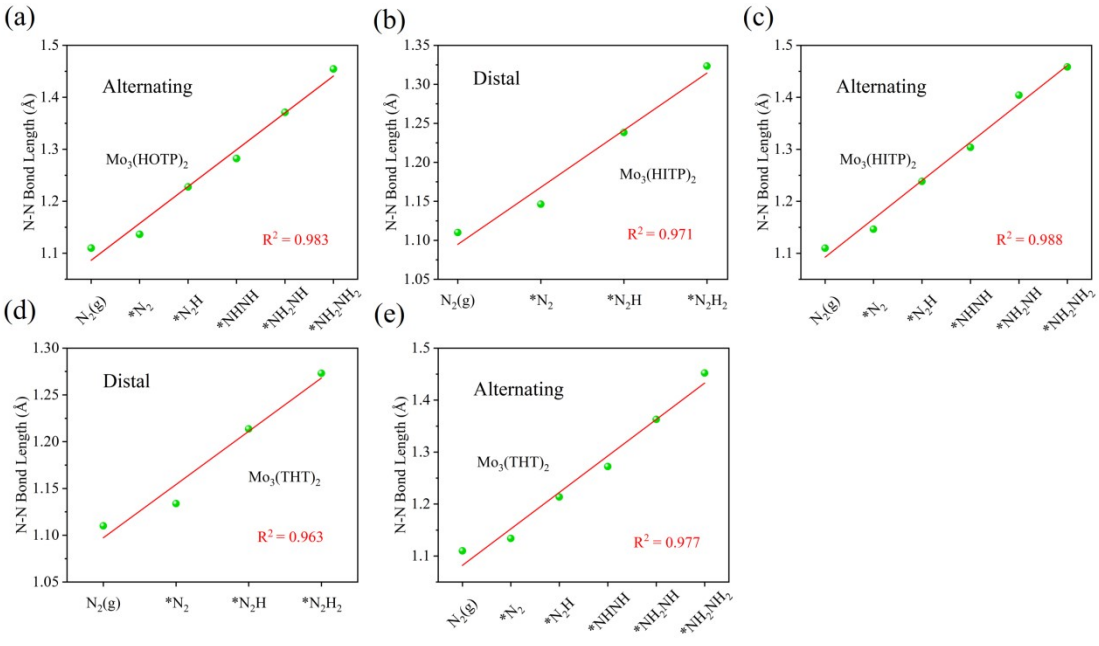

Figure S13. The N–N length of intermediates on $Mo_3(HOTP)_2$, $Mo_3(HITP)_2$ and $Mo_3(THT)_2$ surface through the (b, d) distal and (a, c, e) alternating pathways.

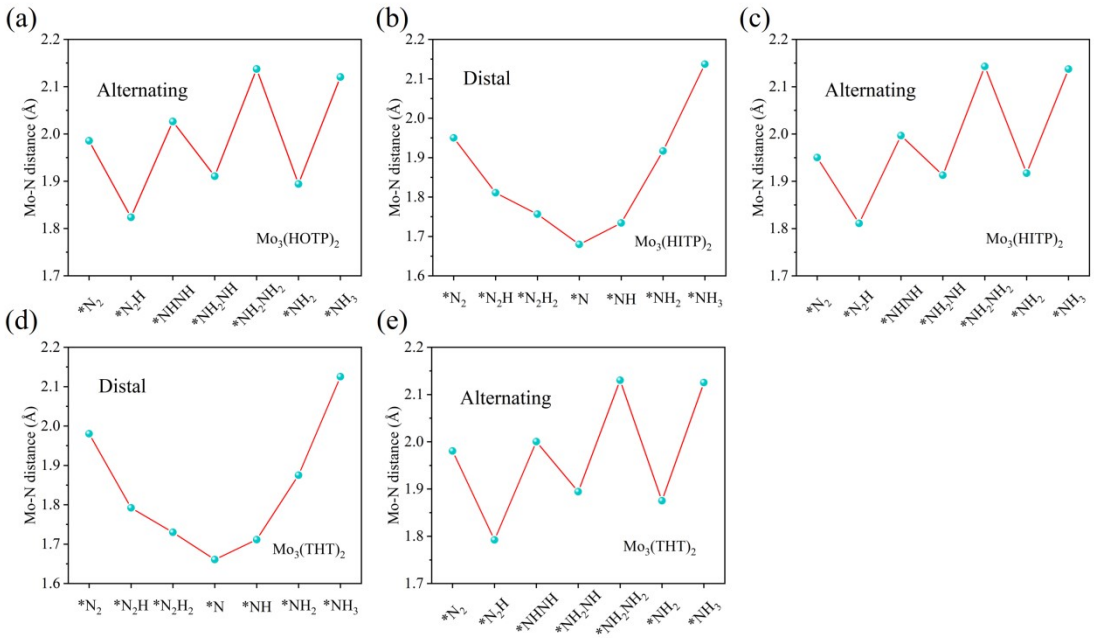

Figure S14. The distances of Mo–N of intermediates on $Mo_3(HOTP)_2$, $Mo_3(HITP)_2$ and $Mo_3(THT)_2$ surface through the (b, d) distal and (a, c, e) alternating pathways.

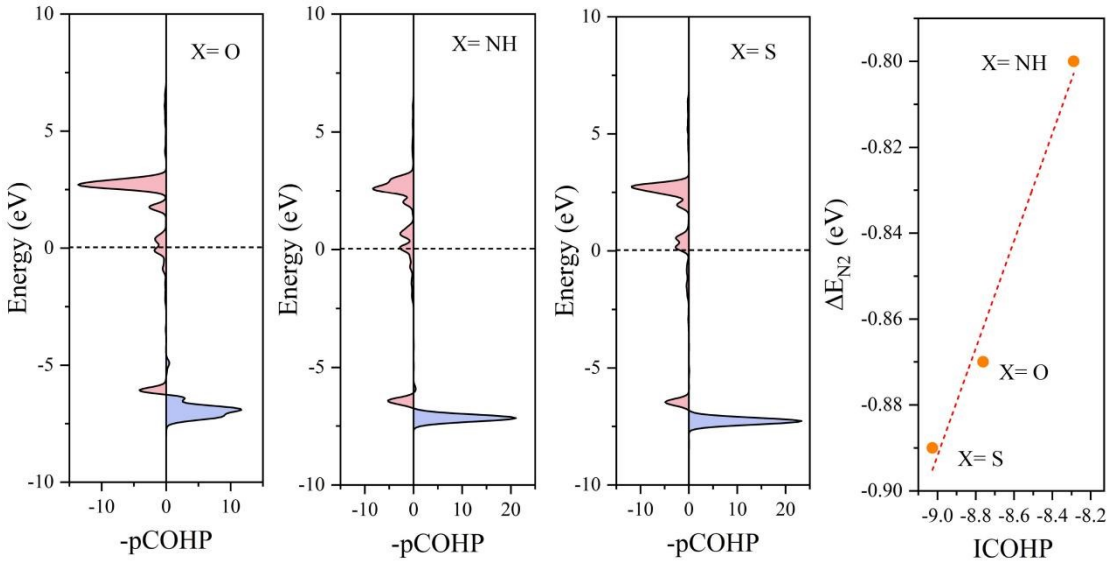

Figure S15. (a-c) The projected crystal orbital Hamilton population (pCOHP) in the $*N_2$. The bonding and antibonding contributions are depicted by pink and blue, respectively. (d) Linear scaling relation between integrated crystal orbital Hamilton population (ICOHP) and adsorption free energy of N_2 (ΔE_{N_2}) of three 2D-CCFs monolayers.

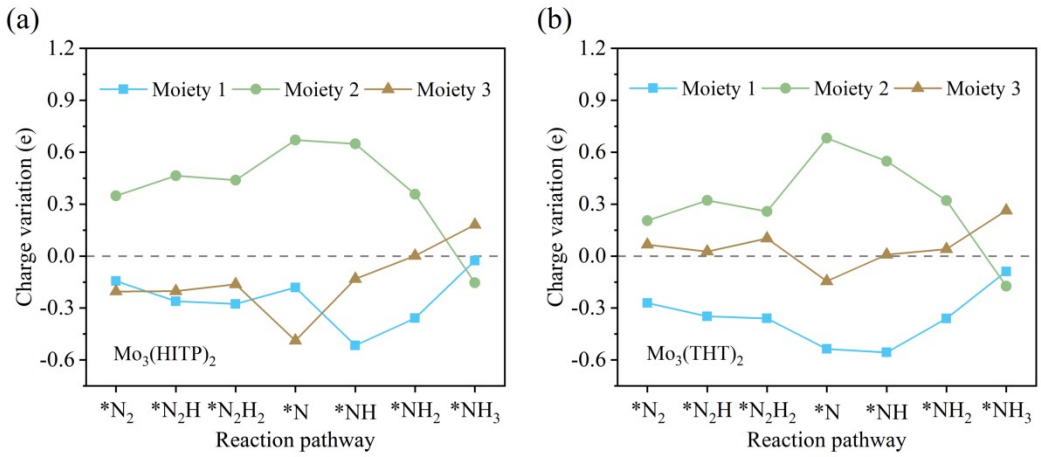

Figure S16. Variation in charge transfer between these moieties along the distal pathway on the (a) $Mo_3(HITP)_2$ and (b) $Mo_3(THT)_2$ monolayers.

Table S1. Lattice parameters, pore size, distance between two adjacent Mo atoms, formation energy (E_f) and the dissolution potential (U_{diss}) of $Mo_3(HOTP)_2$, $Mo_3(HITP)_2$ and $Mo_3(THT)_2$ monolayer.

	Lattice (Å)	D_p (Å)	D_{Mo} (Å)	E_f (eV)	U_{diss} (eV)
$Mo_3(HOTP)_2$	22.39	19.94	11.20	-3.83	1.08
$Mo_3(HITP)_2$	22.74	18.14	11.37	-4.30	1.23
$Mo_3(THT)_2$	24.02	20.82	12.01	-3.71	1.04

Table S2. The values of the Gibbs free energy change of intermediates on $Mo_3(HOTP)_2$, $Mo_3(HITP)_2$ and $Mo_3(THT)_2$ monolayer through the distal pathway.

Adsorption species	ΔG (eV)		
	$Mo_3(HOTP)_2$	$Mo_3(HITP)_2$	$Mo_3(THT)_2$
$*\rightarrow*N_2$	-0.39	-0.29	-0.39
$*N_2\rightarrow*N_2H$	0.41	0.46	0.52
$*N_2H\rightarrow*N_2H_2$	-0.39	-0.12	-0.54
$*N_2H_2\rightarrow*N+NH_3$	-0.49	-0.51	0.09
$*N\rightarrow*NH$	-0.66	-0.73	-1.12
$*NH\rightarrow*NH_2$	-0.15	-0.58	-0.52
$*NH_2\rightarrow*NH_3$	-0.45	0.27	-0.60
$*NH_3\rightarrow*+NH_3$	1.44	0.82	1.88

Table S3. The values of the Gibbs free energy change of intermediates on $Mo_3(HOTP)_2$, $Mo_3(HITP)_2$ and $Mo_3(THT)_2$ monolayer through the alternating pathway.

Adsorption species	ΔG (eV)		
	$Mo_3(HOTP)_2$	$Mo_3(HITP)_2$	$Mo_3(THT)_2$
$*\rightarrow*N_2$	-0.39	-0.29	-0.39
$*N_2\rightarrow*N_2H$	0.41	0.46	0.52
$*N_2H\rightarrow*NHNH$	0.33	0.34	0.13
$*NHNH\rightarrow*NH_2NH$	-0.83	-0.71	-0.75
$*NH_2NH\rightarrow*NH_2NH_2$	0.12	0.42	-0.23
$*NH_2NH_2\rightarrow*NH_2+NH_3$	-1.31	-1.99	-1.24
$*NH_2\rightarrow*NH_3$	-0.45	0.27	-0.60
$*NH_3\rightarrow*+NH_3$	1.44	0.82	1.88

Table S4. The values of the Gibbs free energy change of intermediates on $Mo_3(HOTP)_2$, $Mo_3(HITP)_2$ and $Mo_3(THT)_2$ monolayer through the enzymatic pathway.

Adsorption species	ΔG (eV)		
	$Mo_3(HOTP)_2$	$Mo_3(HITP)_2$	$Mo_3(THT)_2$
$*\rightarrow*N_2$	0.15	0.26	0.27
$*N_2\rightarrow*N_2H$	0.18	0.19	-0.04
$*N_2H\rightarrow*NHNH$	-0.11	-0.32	-0.51
$*NHNH\rightarrow*NH_2NH$	-0.85	-0.59	-0.45
$*NH_2NH\rightarrow*NH_2NH_2$	-0.18	-0.73	-0.46
$*NH_2NH_2\rightarrow*NH_2+NH_3$	-0.86	-0.58	-0.77
$*NH_2\rightarrow*NH_3$	-0.45	0.27	-0.60
$*NH_3\rightarrow*+NH_3$	1.44	0.82	1.88

Table S5. Comparison of electrocatalytic activities for NRR of the Mo3(HOTP)2 catalyst and recently reported 2D-CCFs composites.

Catalyst	Transition metal	Linkers	Limit potential (V)	Reference
$Mo_3(HOTP)_2$	Mo	hexa-substituted triphenylene	-0.41	This work
$W_3(HAT)_2$	W	1,4,5,8,9,12-hexaazatriphenylene	-0.45	1
MPc	Mo/Tc	Phthalocyanine	-0.33/-0.54	2
2D Mo−Pp	Mo	porphyrin (Pp) sheets	-0.58	3
$Mo_3(C_6X_6)_2$	Mo	hexa-substituted benzene	-0.37	4
$W_3C_{12}O_{12}$	W	C_6O_6	-0.59	5
$TM_3(HHTT)_2$	Mo	2,3,7,8,12,13-hexahydroxy tetraazanaphthotetraphene	-0.60	6
TM – PTC	Fe	1,2,3,4,5,6,7,8,9,10,11,12-perthiolated coronene	-0.53	7
$TM_3(C_2O)_{12}$	Mo	1,2,3,4,5,6,7,8,9,10,11,12-perthiolated coronene	-0.36	8

Table S6. The Bader charge analyzed charge transfer (|*e*|) between the three moieties of $Mo_3(HOTP)_2$ for NRR along the distal pathway.

Adsorption species	Moiety 1	Moiety 2	Moiety 3
$*N_2$	–0.25	0.28	–0.02
$*N_2H$	–0.31	0.35	–0.04
$*N_2H_2$	–0.46	0.30	0.16
*N	–0.46	0.72	–0.26
*NH	–0.57	0.52	0.05
$*NH_2$	–0.42	0.23	0.19
$*NH_3$	–0.11	–0.20	0.31

Table S7. The Bader charge analyzed charge transfer (|*e*|) between the three moieties of $Mo_3(HITP)_2$ for NRR along the distal pathway.

Adsorption species	Moiety 1	Moiety 2	Moiety 3
$*N_2$	–0.14	0.34	–0.20
$*N_2H$	–0.26	0.46	–0.20
$*N_2H_2$	–0.27	0.43	–0.16
*N	–0.18	0.67	–0.48
*NH	–0.51	0.64	–0.13
$*NH_2$	–0.35	0.35	0.01
$*NH_3$	–0.02	–0.15	0.18

Table S8. The Bader charge analyzed charge transfer (|*e*|) between the three moieties of $Mo_3(THT)_2$ for NRR along the distal pathway.

Adsorption species	Moiety 1	Moiety 2	Moiety 3
$*N_2$	–0.27	0.20	0.06
$*N_2H$	–0.34	0.32	0.02
$*N_2H_2$	–0.35	0.25	0.10
*N	–0.53	0.68	–0.14
*NH	–0.55	0.54	0.01
$*NH_2$	–0.36	0.32	0.04
$*NH_3$	–0.08	–0.17	0.26

Reference:

1. C. Wang, X. Zhou, and Y. Li, *2D Materials*, 2023, **10**, 024002.
2. C.-X. Huang, G. Li, L.-M. Yang and E. Ganz, *ACS Appl. Mater. Interfaces*, 2021, **13**, 608−621.
3. S. Liu, Y. Liu, X. Gao, Y. Tan, Z. Cheng, Z. Shen and M. Fan, *J. Phys. Chem. C*, 2020, **124**, 1492−1499.
4. J. Zhang, X. Zhu, W. Geng, T. Li, M. Li, C. Fang, X. Shan, Y. Li and Y. Jing, *J. Energy Chem.*, 2021, **61**, 71−76.
5. R. Wang, C. He, W. Chen, L. Fu, C. Zhao, J. Huo and C. Sun, *Nanoscale*, 2021, **13**, 19247−19254.
6. Y. Sun, W. Shi, M. Sun, Q. Fang, X. Ren, Y. Yan, Z. Gan, Y.-Q. Fu, A. Elmarakbi, Z. Li and Z. Wang, *Int. J. Hydrog. Energy*, 2023, **48**, 19972−19983.
7. B. Li, W. Du, Q. Wu, Y. Dai, B. Huang and Y, Ma. *The Journal of Physical Chemistry C*, 2021, **125**, 20870−20876.
8. Z. Feng, Z. Yang, X. Meng, F. Li, Z. Guo, S. Zheng, G. Su, Y. Ma, Y. Tang and X. Dai, *J. Mater. Chem. A*, 2022, **10**, 4731−4738.